Desalination and Water Treatment
www.deswater.com

doi: 10.5004/dwt.2019.24329

162 (2019) 134–141
September

Breakthrough modelling of glucamine functionalized PVDF nanofibrous adsorbent in a fixed-bed column for separation of boron from water

Madana Leela Nallappan[a], Mohamad Mahmoud Nasef[b,*], Teo Ming Ting[c], Arshad Ahmad[d]

[a]*Faculty of Chemical Engineering, Universiti Teknologi Malaysia, 81310 Johor Bahru, Johor, Malaysia, email: madanaleela87@gmail.com*
[b]*Chemical Engineering Department, Universiti Teknologi PETRONAS, 32610 Seri Iskander, Perak, Malaysia, Tel. +305-3657561; emails: mohamed.nasef@utp.edu.my, mahmoudeithar@cheme.utm.my (M.M. Nasef)*
[c]*Radiation Technology Division, Malaysian Nuclear Agency, 43000 Kajang, Selangor, Malaysia, email: tmting@nm.gov.my*
[d]*Center of Hydrogen Energy, Institute of Future Energy, Universiti Teknologi Malaysia, 81310 Johor Bahru, Johor, Malaysia, email: arshad@utm.my*

Received 1 January 2019; Received 24 April 2019

ABSTRACT

The performance of new nanofibrous chelating adsorbent, prepared by radiation induced grafting of glycidyl methacrylate onto electrospun poly(vinylidene fluoride) (PVDF) nanofibers followed by functionalization with *N*-methyl-*D*-glucamine, for removal of boron from aqueous solutions using a fixed-bed column was evaluated. The breakthrough curve was studied under various parameters including initial concentration, flow rate and bed height at pH 7. The column performance was evaluated with Yoon–Nelson and Thomas adsorption kinetic models. The maximum performance for boron adsorption was obtained at an initial concentration of 10 mg L^{-1}, a space velocity (SV) of 15 h^{-1} and a room temperature of 28°C. The breakthrough capacity was found to be a function of both initial feed concentration and flow rate. Thomas model was found to best fit the dynamic behaviour of the column. The newly obtained adsorbent was proven to be capable of removing boron efficiently from aqueous solutions in continuous fixed-bed systems at high flow rates and has potential for industrial-scale application.

Keywords: Nanofibrous boron-selective adsorbent; Breakthrough curve; Adsorption kinetic models; Fixed-bed column

1. Introduction

The growing environmental and health concerns over the rise of boron concentration in surface and waste water streams is prompting the development of new materials and systems for efficient treatment of the contaminated streams [1,2]. The surface water gets contaminated by boron through leakages of urban wastewater containing detergents and cleaning products [3]. On the other hand, the growing use of boron in various industries (e.g., heat-resistant materials, ceramics, glass, dyestuff, fertilizers and food preservatives) led to contamination rise in industrial wastewaters [4]. Thus, a stringent control over boron concentrations in drinking, irrigation and waste waters has been imposed by environmental authorities in many countries. A value of 2.4 mg B L^{-1} was set by WHO for drinking water [5] whereas <4.0 mg B L^{-1} was set for discharged wastewater in various countries [6]. Nevertheless, the irrigation water was set at far lower value (0.5 mg B L^{-1}) to prevent plant toxicity [7].

Boron compounds are mostly present in water streams in boric acid form unlike seawater where boron is in a form of negatively charged borate ions that can be easily

* Corresponding author.

removed by soluble ions separation technology (e.g., reverse osmosis) [8,9]. Technologies such as adsorption–coagulation [10], electro-coagulation [11], electrodialysis [12], reverse osmosis [13,14] and ion chelation with resins [2,15–17] have been considered for boron removal from various solutions [1,18,19]. Off all, boron removal by selective adsorption with chelating resins is the most attractive technology for capturing neutral boron from various streams. Particularly, *N*-methyl-*D*-glucamine (NMDG) containing resins showed high boron selectivity and ability to bring its concentration in solutions to few milligrams per liter [4]. The change of granular resins to fibrous structures increased the boron removal efficiency which was prompted by higher adsorption capacity and faster kinetics [20,21]. The fibrous chelating adsorbents with enhanced performance were conveniently prepared by radiation induced grafting (RIG) and subsequent functionalization with NMDG [22,23]. For example, adsorbents with fibrous substrates of polyethylene/polypropylene (PE-PP) and nylon-6 were grafted with glycidyl methacrylate (GMA) [24] and vinylbenzyl chloride [6] and subsequently treated with NMDG. Both adsorbents showed higher boron adsorption capacity twofolds faster kinetics than commercial resins [24]. Nonetheless, there is a room to enhance the mass transfer and overcome the surface area limitation of the micro-fibrous boron selective adsorbents by using nanofibers substrates with their small interfibrous pore size, high permeability with large surface area per unit mass. This is likely to further reduce the diffusion path of boron ions and provide more chelation sites for enhancing boron adsorption. A new adsorbent was prepared by RIG of GMA onto electrospun poly(vinylidene fluoride) (PVDF) nanofibers followed by immobilization of NMDG. The nanofibrous adsorbent with fine fibres diameters (500 ± 100 nm) and NMDG density of 2.2 mmol g^{-1}-adsorbent achieved the highest adsorption capacity at pH of 7 under static conditions [25]. However, there is no reports on performance of such nanofibrous adsorbent in a fixed-bed system for potential industrial-scale removal of boron from water streams.

The objective of this study is to evaluate the performance of NMDG-containing nanofibrous adsorbent for removal of boron from aqueous solutions under dynamic conditions using column adsorption method. The effects of system parameters such as boron concentration, flow rate and bed height on the breakthrough curve were investigated. The shape of breakthrough curve was analyzed to correlate the solid phase loading and exhaustion time of the bed. The column kinetics was analyzed using Yoon–Nelson and Thomas models. The column regeneration and reusability were also evaluated in three cycles.

2. Methodology

2.1. Materials

PVDF powder was supplied by Sigma-Aldrich (Milwaukee, WI, USA) (Mw = 534,000, d = 1.74 g cm^{-3}, mp = 165°C). *N*,*N*-dimethylformamide (DMF, 99.5%) and acetone (99.7%) were purchased form Merck (Darmstadt, Germany). GMA (monomer purity ≥99%) and tetrahydrofuran (anhydrous, ≥99.9%) were supplied by Sigma-Aldrich (Milwaukee, WI, USA). Ethanol, propanol, methanol, and butanol (EMSURE® ACS) were obtained from Merck Millipore. NMDG (purity ≥ 99%) was purchased from Sigma-Aldrich. All chemicals were used as received without any further purification. Deionized water (DI) obtained from a water purifier (NANOpure Diamond™) was used to prepare boron solution with concentration of 1,000 mg L^{-1} by dissolving 5.716 g of H_3BO_3 in DI and diluted to 1,000 mL and used as a stock solution to prepare various solutions with desired concentrations. The pH of the solution was adjusted using HCl (1 M) and NaOH (1 M) solutions.

2.2. Preparation of nanofibrous adsorbent

PVDF solution of 15 wt.% concentration was prepared by dissolving the polymer powder in a mixture of DMF and acetone at 8:2 (v/v) ratio under continuous stirring for an hour at 70°C. The PVDF solution was electrospun using electrospinning system operating at 0.3 mL h^{-1} flow rate, 14.5 kV voltage, 25°C temperature and 15 cm tip-to-collector distance following the procedure reported elsewhere [26].

The PVDF nanofibrous samples were immersed in a beaker containing 10% GMA in methanol for 12 h. The GMA saturated samples were transferred into PE zipper locked bag and deaerated with N_2 gas to remove oxygen. The samples were irradiated to a total dose of 100 kGy using an EB accelerator (EPS 3000) with an accelerating voltage of 1.0 MeV and beam current of 10 mA. The grafted samples were extracted and washed repeatedly using methanol to remove the remaining monomer and any formed homopolymer. The grafted fibers were dried using a vacuum oven for 20 h at 50°C and their increase in weight was calculated. The degree of grafting (DG) was determined using the following equation:

$$\mathrm{DG}(\%) = \frac{W_g - W_0}{W_0} \times 100 \quad (1)$$

where W_0 and W_g are the weights before and after grafting, respectively.

Poly(GMA) grafted PVDF nanofibrous samples with 150% DG were treated with NMDG under continuous stirring and reflux at optimum reaction parameters of 15% NMDG concentration, 87.0°C temperature, 65 min time as reported in a previous study [25]. The NMDG-containing nanofibers were washed with DI few times and dried under vacuum for 20 h at 40°C. The density of NMDG group in the adsorbent was calculated according to the following formula:

$$\text{Density of glucamine}\left(\frac{\text{mmol}}{\text{g, adsorbent}}\right) = \frac{\left(\frac{Z_f - Z_i}{Z_f}\right)}{M} \times 1000 \quad (2)$$

where Z_i and Z_f are the weights of the initial grafted fibers and final functionalized fibers whereas M is the molecular weight of NMDG.

2.3. Column adsorption studies

A column made of Pyrex glass with a length of 5 cm and an internal diameter of 1 cm was filled with 0.687 g

(0.785 mL) of the nanofibrous adsorbent and the top and bottom of the column were covered with glass beads and glass wool layers, respectively. Boric acid solutions with concentrations of 10, 30 and 60 mg L^{-1} were introduced upward to the column by a peristaltic pump at desired flow rates with fresh adsorbent bed used for every flow rate. All experiments were carried out at room temperature and pH 7 at which the maximum adsorption for grafted NMDG/poly(GMA) moieties takes place [20,25]. Samples from the column effluent were collected at regular times using a fractionating collector and the experiments were ended after the adsorbent in the column reached a complete exhaustion. Boron concentration in the effluent samples was determined using inductively coupled plasma-optical emission spectroscopy (ICP-OES, PerkinElmer-Optima 7300 DV, USA) operated at a plasma gas flow of 15 L min^{-1}, auxiliary gas flow of 0.5 L min^{-1}, nebulizer gas flow of 0.7 L min^{-1} and pump rate of 0.5 L min^{-1}. Standard solutions of boron (0.1, 1.0, 3.0, 5.0, 8.0 and 10.0 mg L^{-1}) were used to prepare the calibration curve, which was linear with a correlation coefficient of above 0.999. The bed volume (BV, mL sample solution/mL nanofibrous adsorbent) was calculated using the following equation:

$$\mathrm{BV} = \frac{Q_t}{V} \tag{3}$$

where Q is the flow rate of feed solution (mL min^{-1}), t is the operating time of adsorption in column (min) and V is the volume of the wet adsorbent (mL).

The space velocity (SV, h^{-1}) was obtained by dividing the flow rate of the boric acid solution over the nanofibrous adsorbent wet volume packed in the column using Eq. (4):

$$\mathrm{SV} = \frac{Q}{V} \tag{4}$$

The breakthrough point was calculated according to Eq. (5):

$$\frac{C_1}{C_0} = 0.05 \tag{5}$$

where C_0 and C_1 are the influent and effluent boron concentrations, respectively.

The effect of bed height was also studied by varying the bed heights in the range of 0.5–1.5 cm.

The adsorbed boron in the column was eluted with 1 M HCl solution at the same flow rate applied for the adsorption [20]. The elution efficiency is obtained by Eq. (6):

$$\text{Elution efficiency}(\%) = \frac{\text{Amount of eluted boron}(\text{mg})}{\text{Amount of adsorbed boron}(\text{mg})} \times 100 \tag{6}$$

The obtained adsorption data were fitted to Thomas and Yoon–Nelson kinetic models to study the kinetic adsorption behaviour and breakthrough performance of the fixed-bed column.

3. Result and discussion

3.1. Nanofibrous adsorbent properties

The new nanofibrous boron chelating adsorbent showed a combination of properties as summarized in Table 1.

3.2. Evaluation of boron adsorption under fixed-bed column conditions

3.2.1. Effect of initial boron concentration

Fig. 1 shows the effect of initial boron concentration on the breakthrough curves. The breakthrough volume (V_B) decreased from 337.5 to 150 mL and the saturation volume (V_S) decreased from 600 to 387.5 mL with the increase in initial boron concentrations from 10 to 60 mg L^{-1}, which has also made slope of the breakthrough curve steeper. Bearing in mind that the main driving force for the adsorption is the concentration difference between the solute in the solution and that in the adsorbent, this behaviour can be attributed to high concentration differences, which provide higher driving force favouring adsorption process [27].

3.2.2. Effect of solution flow rates

Breakthrough curves for boron adsorption at different feed flow rates, that is, various SV values (15, 50, 100 and 200 h^{-1}) are presented in Fig. 2. The breakthrough curves were observed to become steeper and reached faster saturation with the increase in the flow rate. This trend is mostly due to the decrease in the contact time between the adsorbent and adsorbate leading to a parallel decrease in the treated volume causing an early breakthrough. This was confirmed by the data shown in Table 2 revealing an obvious decrease in both V_B and V_S from 337.5 and 600 mL to 250 and 400 mL with the rise in the flow rate from 15 to 200 h^{-1}, respectively.

The breakthrough point capacity and total saturation capacity of the breakthrough curves obtained at various flow rates are presented in Fig. 3. The breakthrough capacity barely changed with the increase in SV from 15 to 200 h^{-1}. This behaviour is caused by the presence of a large number of adsorption sites on the adsorbent, which mitigate the high diffusion rate imparted by short diffusion path in the nanofibrous structure of the adsorbent. This suggests that the nanofibrous adsorbent has the potential to remove boron at high flow rates with high performance.

Table 1
Properties of the prepared fibrous boron chelating adsorbent

Properties	Nanofibrous chelating adsorbent
Base material	PVDF nanofibers
Moiety	NMDG
Chemical structure	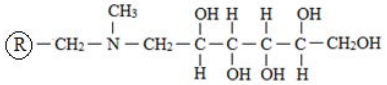
Density of NMDG	2.20 mmol g^{-1}-adsorbent
Water content	30%–40%
Average fiber diameter	ca. 500 ± 100 nm

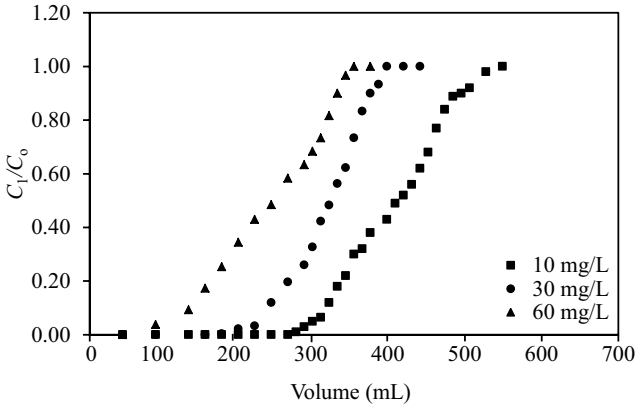

Fig. 1. Effect of initial concentration on breakthrough curves. Experiment conditions are pH, 7; SV, 15 h^{-1}; bed height, 1 cm and temperature, 28°C.

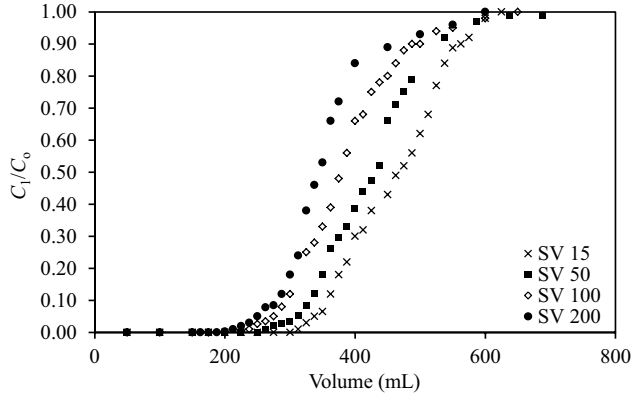

Fig. 2. Effect of flow rate on the breakthrough curve at different space velocities. Conditions are pH, 7; initial concentration, 10.0 mg L^{-1} and bed height, 1 cm and temperature, 28°C.

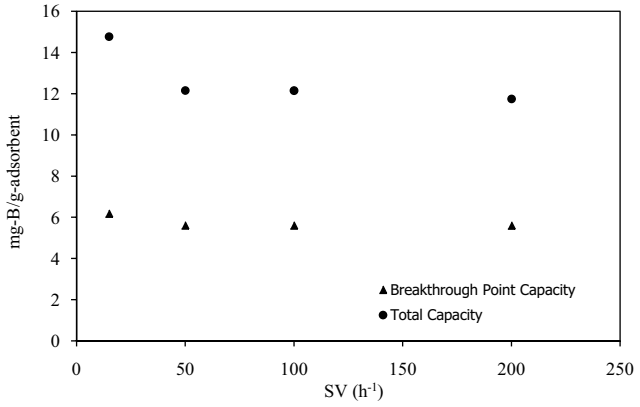

Fig. 3. Variation of breakthrough point capacity and total capacity with space velocity. Experiment conditions are as in Fig. 2.

On the other hand, the total saturation capacity was reduced from 14.76 to 12.17 mg B g^{-1}-adsorbent with the increase in the SV from 15 to 50 h^{-1} beyond which no significant change took place with further increase in SV up to 200 h^{-1}. The initial reduction in the total capacity is due to the decrease in the contact time despite the large surface area and this is likely caused by partial restriction on the boron interaction with the adsorbent to small extent. However, the nanofibrous adsorbent performance remained remarkably high even at very high flow rates and therefore, the present adsorbent is confirmed to have high potential for application in boron removal at high feed flow rates.

3.2.3. Effect of nanofibrous adsorbent bed height

Fig. 4 shows the breakthrough curves for boron adsorption of the nanofibrous adsorbent evaluated at an initial boron concentration of 10 mg L^{-1}, pH 7 and flow rate of SV 15 h^{-1}. As can be seen, the bed height significantly affected the column performance. Table 2 shows an increase in both V_B and V_S values with the increase in the bed height and such an increase is likely to be due to the increase in the adsorbent dosage caused by the increase in the bed height providing more active sites for adsorption to occur. The increase in the bed height of the column raised contact time and resulted in an increase in the binding sites available for boron adsorption and this agrees very well with the literature [28–30]. A summary of the effect of variation of the initial boron concentrations, flow rates and bed heights on the performance of the column are presented in Table 2.

3.3. Yoon–Nelson model

The Yoon and Nelson equation is expressed as follows [31–33]:

$$\frac{C}{C_0}=\frac{\exp\left(K_{YN}t-\tau K_{YN}\right)}{1+\exp\left(K_{YN}t-\tau K_{YN}\right)} \tag{7}$$

where K_{YN} is the rate constant (min^{-1}), and τ is the time required for 50% adsorbate breakthrough (min) when C (mg L^{-1}) is one-half of C_0. As stated by the Yoon and Nelson model, the rate constant characterizes the shape of the breakthrough curve. A sharp breakthrough curve always has a large rate constant [31–33]. The linearized form of the Yoon and Nelson model is described as follows:

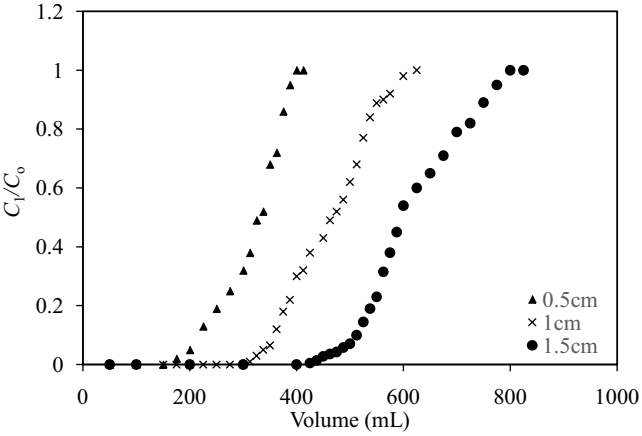

Fig. 4. Effect of bed height on the breakthrough curve at different bed heights. Conditions are pH, 7; initial concentration, 10 mg L^{-1}; SV, 15 h^{-1} and temperature, 28°C.

Table 2
Summary of column performance data for different initial boron concentrations, flow rates and bed heights

Parameters	Values	V_B (mL)	V_S (mL)
C_0 (mg L^{-1})	10	337.5	600.0
	30	225.0	437.5
	60	150.0	387.5
SV (h^{-1})	15	337.5	600.0
	50	312.5	587.5
	100	275.0	500.0
	200	250.0	400.0
Bed height (cm)	0.5	200.0	400.0
	1.0	337.5	600.0
	1.5	425.0	750.0

$$\ln\frac{C}{C_0 - C} = K_{YN}t - \tau K_{YN} \tag{8}$$

K_{YN} and τ values can be determined from ln (C/(C_0−C)) against t plots. Based on the model, the amount of boron adsorbed is one half of the initial (inlet) boron concentration passed through the fixed-bed column within the 2τ period. Therefore, the following equation can be written to provide the sorption capacity, q_0 (mg g^{-1}), where Q represents the volumetric flow rate (L min^{-1}) while m represents the mass of sorbent (g) [31–33]:

$$q_0 = \frac{0.5\left[C_0 Q(2\tau)\right]}{m} = \frac{C_0 Q\tau}{m} \tag{9}$$

The calculated parameters, K_{YN} (rate constant) and τ (the time required for 50% boron breakthrough), at different conditions of initial boron concentration, flow rate and bed height are listed in Table 3. The K_{YN} value generally decreases with the increase in the initial boron concentrations whereas, τ increases due to the rapid saturation of the column with the increase in the inlet boron concentration. Furthermore, the value of τ increases while that of K_{YN} decreases with the increase in bed height.

The correlation coefficients (R^2) between the experimental and predicted values obtained using Yoon–Nelson model for all tested flow rates were between 0.8278 and 0.9778 for all experimental conditions and the sum of squares (SS) was greater than 0.0185 for almost all conditions. The comparison between the experimental and predicted curves according to the Yoon–Nelson model at different conditions is shown in Fig. 5. The experimental breakthrough curves apparently did not show a good fit with the predicted counterparts from the model. This suggests that Yoon–Nelson model is not adequate for describing the kinetic adsorption behaviour of boron onto the NMDG-containing nanofibrous adsorbent.

3.4. Thomas model

The Thomas model is represented by following equation [33–35]:

$$\frac{C}{C_0} = \frac{1}{1 + \exp\left(K_T \dfrac{\left(q_e m - C_0 V\right)}{Q}\right)} \tag{10}$$

where K_T is the Thomas rate constant (mL min^{-1} mg^{-1}), Q is the volumetric flow rate (L min^{-1}), m is the mass of the adsorbent (g) and V is the volume of the solution passed through the column at any time. C (mg L^{-1}) and q_e (mg g^{-1}) each represents the adsorbate concentration and the adsorption capacity, respectively. The linearized form of the Thomas model is given as follows:

$$\ln\left(\frac{C}{C_0} - 1\right) = \frac{K_T q_e m}{Q} - \frac{K_T C_0}{Q} \times V \tag{11}$$

K_T and sorption capacity, q_e, can be determined from the plot of ln [(C_0/C)−1] against time (V/Q). Error analysis was performed by analyzing SS of the differences between the experimental and the theoretical data obtained from the model. The relative mathematical formula of SS of error can be acquired in the following equation [34]:

Table 3
Yoon–Nelson model constants at different initial boron concentrations, flow rates and bed height

Parameters	Values	K_{YN} (L min^{-1})	τ (h)	q_0 (mg g^{-1})	R^2	SS
C_0 (mg L^{-1})	10	0.5268	20.9	6.8576	0.9568	0.0460
	30	0.6945	21.6	21.2005	0.9778	0.0929
	60	0.3725	46	92.1651	0.9654	0.2867
SV (h^{-1})	15	0.5268	20.9	6.8576	0.9568	0.0460
	50	1.6273	5.8	6.0187	0.9623	0.0369
	100	3.779	2.7	5.9199	0.8278	0.0185
	200	7.219	1.2	5.3039	0.9340	0.0220
Bed height (cm)	0.5	0.5998	14	9.298	0.8469	0.0956
	1	0.5268	20.9	6.8576	0.9568	0.0460
	1.5	0.4617	27.7	6.1233	0.9606	0.0643

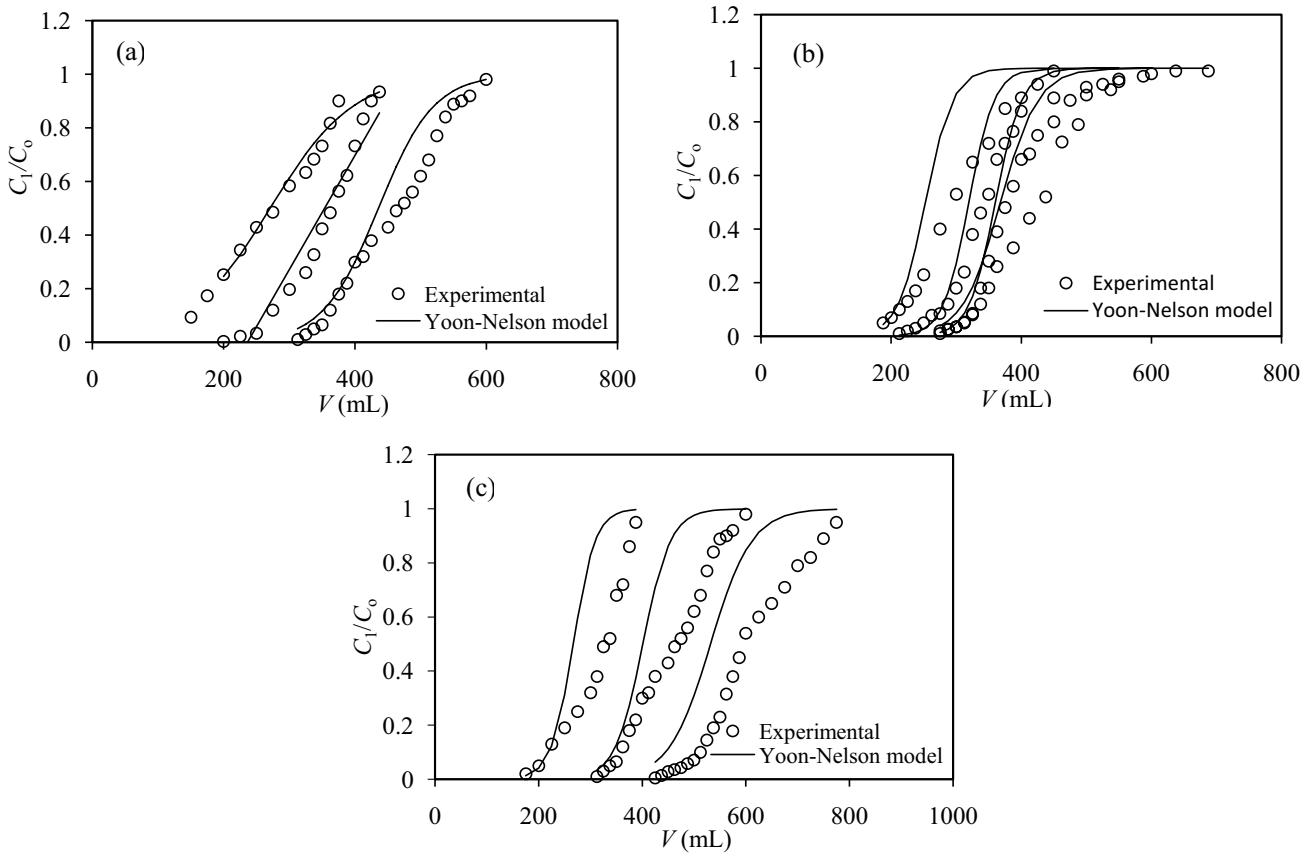

Fig. 5. Yoon–Nelson model curves at different (a) initial concentrations, (b) flow rates and (c) bed heights.

$$\mathrm{SS} = \frac{\sum\left[\left(\frac{C_1}{C_0}\right)_c - \left(\frac{C_1}{C_0}\right)_e\right]^2}{N} \tag{12}$$

where $(C_1/C_0)_c$ is the ratio of effluent and initial boron concentrations obtained from calculation according to the dynamic models, and $(C_1/C_0)_e$ is the ratio of the effluent and initial boron concentrations acquired from experiment, respectively. N is the number of the experimental points. The best fitting isotherm for the adsorption system was confirmed by fitting data using SS combined with the values of the determined coefficient (R^2). The column data were fitted to Thomas model to determine the Thomas rate constant (K_T) and maximum adsorption capacity (q_e). A non-linear regression analysis was used to evaluate the data fitting to Thomas model. The calculated parameters for different conditions of the initial boron concentration, flow rate and bed height are listed in Table 4. The correlation coefficient (R^2) values ranged

Table 4
Thomas model constants at different initial boron concentrations, flow rates and bed heights

Parameters	Values	K_T (L mg^{-1} min^{-1})	q_e (mg g^{-1})	R^2	SS
C_0 (mg L^{-1})	10	0.8886	6.3429	0.9803	0.0113
	30	0.3563	15.0614	0.9876	0.0074
	60	0.1171	22.5068	0.9932	0.0065
SV (h^{-1})	15	0.6166	6.5724	0.9958	0.0035
	50	2.5641	6.0187	0.9923	0.0019
	100	7.404	5.4964	0.9878	0.0028
	200	15.3712	4.9625	0.9940	0.0012
Bed height (cm)	0.5	1.0644	8.5102	0.9969	0.0306
	1	0.8459	6.3401	0.9903	0.0108
	1.5	0.5679	5.7977	0.9906	0.0028

from 0.9803 to 0.9969. The values of SS were found to be low indicating a good agreement between the experimental data and the theoretical data generated using Thomas model.

Figs. 6a–c depict the breakthrough curves for the experimental data and the model data generated using Thomas model at different experimental conditions. The comparison between the experimental and predicted breakthrough curves shows a good fit. This indicates that the external and internal diffusions are not the rate limiting step.

The value of q_e was found to decrease, while the Thomas rate constant K_T increased with the increase in flow rate. The increase in rate constant (K_T) indicates that the mass transport resistance has a decreasing trend [27]. As the bed height increased, both the values of q_e and K_T were found to decrease. The low SS values together with the close agreement noticed in Fig. 6 further confirms that the breakthrough curves of Thomas model demonstrated a better agreement with the experimental data than Yoon–Nelson model. It can be concluded that boron adsorption behaviour of the newly prepared NMDG-containing nanofibrous adsorbent can be best described by Thomas model. Moreover, the external and internal diffusions are not the limiting steps in boron adsorption [36].

3.5. Regeneration of adsorbent

The nanofibrous adsorbent was tested and regenerated in three cycles at 10 mg L^{-1} initial concentration, 15 h^{-1} SV, pH 7, 1 cm bed height and room temperature. No significant reduction in the performance of the bed could be observed even after 3 cycles as indicated by the negligible changes in V_B, V_S and q_0. Particularly, V_B recorded a slight shift from 337.5 to 321.5 coupled with no variation in V_S, which stands at 600 and a minor reduction in q_0 from 13.68 to 13.28 mg g^{-1} after the third cycle. These results indicate that the new nanofibrous adsorbent is highly efficient for the adsorption and desorption and the boron uptake is reversed without significant loss of binding efficiency.

4. Conclusion

A nanofibrous selective boron adsorbent that was prepared by RIG of GMA onto electrospinning nanofibrous PVDF sheets and subsequent functionalization with NMDG was evaluated in a fixed-bed column under different initial concentrations, flow rates and bed heights. The V_B and V_S were found to decrease with the increase in the initial boron concentrations and flow rates whereas they increased with the rise in bed height. Thomas model was found to be adequate for describing the adsorption behaviour of boron on the new glucamine-containing nanofibrous adsorbent compared with Yoon and Nelson kinetic model. The adsorbent was regenerated and used for three cycles without any significant loss in the adsorption efficiency. The overall performance suggests that the nanofibrous adsorbent can achieve high boron removal capacity even at high flow

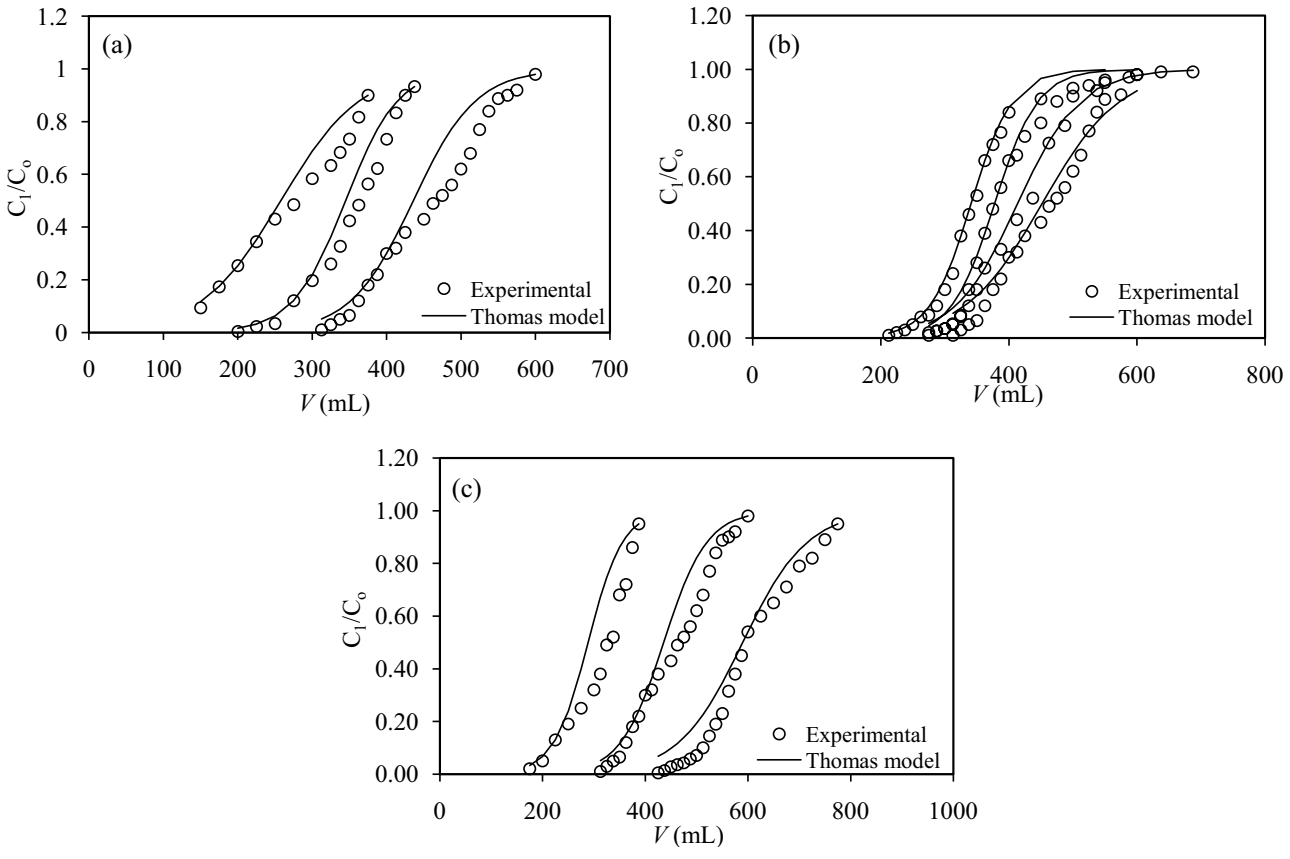

Fig. 6. Thomas model curves at different: (a) initial concentrations, (b) flow rates and (c) bed heights.

rates. It can be finally concluded that the newly prepared nanofibrous adsorbent has a strong potential for practical application in boron removal from solutions.

Acknowledgement

ML Nallappan would like to acknowledge the financial support by Ministry of Higher Education (Malaysia) through FRGS awarded to Universiti Teknologi Malaysia (grant no. 4F878). MM Nasef is grateful to Universiti Teknologi PETRONAS for supporting this work through Y-UTP (cost center. 015LC0-065).

References

[1] N. Hilal, G.J. Kim, C. Somerfield, Boron removal from saline water: a comprehensive review, Desalination, 273 (2011) 23–35.
[2] J. Kluczka, T. Korolewicz, M. Zołotajkin, J. Adamek, Boron removal from water and wastewater using new polystyrene-based resin grafted with glycidol, Water Resour. Ind., 11 (2015) 46–57.
[3] H. Liu, X. Ye, Q. Li, T. Kim, B. Qing, M. Guo, F. Ge, Z. Wu, K. Lee, Boron adsorption using a new boron-selective hybrid gel and the commercial resin D564, Colloids Surf., A, 341 (2009) 118–126.
[4] M.M. Nasef, M. Nallappan, Z. Ujang, Polymer-based chelating adsorbents for the selective removal of boron from water and wastewater: a review, React. Funct. Polym., 85 (2014) 54–68.
[5] WHO, Guidelines for Drinking Water Quality, 4th ed., World Health Organization, Malta, Gutenberg, 2011.
[6] T.M. Ting, M.M. Nasef, K. Hashim, Evaluation of Boron adsorption on new radiation grafted fibrous adsorbent containing *N*-methyl-*D*-glucamine, J. Chem. Technol. Biotechnol., 91 (2016) 2009–2017.
[7] Q. Shi, J.-Q. Meng, R.-S. Xu, X.-L. Du, Y.-F. Zhang, Synthesis of hydrophilic polysulfone membranes having antifouling and boron adsorption properties via blending with an amphiphilic graft glycopolymer, J. Membr. Sci., 444 (2013) 50–59.
[8] M. Palencia, M. Vera, E. Combatt, Polymer networks based in (4-vinylbenzyl)-*N*-methyl-*D*-glucamine supported on microporous polypropylene layers with retention boron capacity, J. Appl. Polym. Sci., 131 (2014) 40653–40653.
[9] E. Güler, C. Kaya, N. Kabay, M. Arda, Boron removal from seawater: state-of-the-art review, Desalination, 356 (2015) 85–93.
[10] M.F. Chong, K.P. Lee, H.J. Chieng, I.I.S. Binti Ramli, Removal of boron from ceramic industry wastewater by adsorption–flocculation mechanism using palm oil mill boiler (POMB) bottom ash and polymer, Water Res., 43 (2009) 3326–3334.
[11] M.H. Isa, E.H. Ezechi, Z. Ahmed, S.F. Magram, S.R.M. Kutty, Boron removal by electrocoagulation and recovery, Water Res., 51 (2013) 113–123.
[12] M. Turek, P. Dydo, B. Bandura-Zalska, Boron removal from dual-staged seawater nanofiltration permeate by electrodialysis, Desal. Wat. Treat., 10 (2009) 60–63.
[13] K.L. Tu, L.D. Nghiem, A.R. Chivas, Boron removal by reverse osmosis membranes in seawater desalination applications, Sep. Purif. Technol., 75 (2010) 87–101.
[14] C. Dominguez-Tagle, V.J. Romero-Ternero, A.M. Delgado-Torres, Boron removal efficiency in small seawater reverse osmosis systems Desalination, 265 (2011) 43–48.
[15] N. Kabay, S. Sarp, M. Yuksel, Ö. Arar, M. Bryjak, Removal of boron from seawater by selective ion exchange resins, React. Funct. Polym., 67 (2007) 1643–1650.
[16] H. Demey, T. Vincent, M. Ruiz, M. Nogueras, A.M. Sastre, E. Guibal, Boron recovery from seawater with a new low-cost adsorbent material, Chem. Eng. J., 254 (2014) 463–471.
[17] X. Zhang, J. Wang, S. Chen, Z. Bao, H. Xing, Z. Zhang, B. Su, Q. Yang, Y. Yang, Q. Ren, A spherical *N*-methyl-*D*-glucamine-based hybrid adsorbent for highly efficient adsorption of boric acid from water, Sep. Purif. Technol., 172 (2017) 43–50.
[18] J. Wolska, M. Bryjak, Methods for boron removal from aqueous solutions — a review, Desalination, 310 (2013) 18–24.
[19] M. Bodzek, The removal of boron from the aquatic environment–state of the art, Desal. Wat. Treat., 57 (2016) 1107–1131.
[20] T.-M. Ting, H. Hoshina, N. Seko, M. Tamada, Removal of boron by boron-selective adsorbent prepared using radiation induced grafting technique, Desal. Wat. Treat., 51 (2013) 2602–2608.
[21] K. Ikeda, D. Umeno, K. Saito, F. Koide, E. Miyata, T. Sugo, Removal of boron using nylon-based chelating fibers, Ind. Eng. Chem. Res., 50 (2011) 5727–5732.
[22] M.M. Nasef, O. Güven, Radiation-grafted copolymers for separation and purification purposes: status, challenges and future directions, Prog. Polym. Sci., 37 (2012) 1597–1656.
[23] M.M. Nasef, T.M. Ting, A. Abbasi, A. Layeghi-Moghaddam, S.S. Alinezhad, K. Hashim, Radiation grafted adsorbents for newly emerging environmental applications, Radiat. Phys. Chem., 118 (2016) 55–60.
[24] T.M. Ting, M.M. Nasef, Modification of polyethylene-polypropylene fibers by emulsion and solvent radiation grafting systems for boron removal, Fiber Polym., 18 (2017) 1048–1055.
[25] M.L. Nallappan, M.M. Nasef, T.M. Ting, A. Ahmad, An optimized covalent Immobilization of glucamine on electrospun nanofibrous poly(vinylidene fluoride) sheets grafted with oxirane groups for higher boron adsorption, Fiber Polym., 19 (2018) 1694–1705.
[26] M.L. Nallappan, M.M. Nasef, Optimization of elecrospinning of PVDF scaffolds fabrication using response surface method, Jurnal Teknologi, 75 (2015) 103–107.
[27] M. Bhaumik, K. Setshedi, A. Maity, M.S. Onyango, Chromium(VI) removal from water using fixed bed column of polypyrrole/Fe_3O_4 nanocomposite, Sep. Purif. Technol., 110 (2013) 11–19.
[28] P.A. Kumar, S. Chakraborty, Fixed-bed column study for hexavalent chromium removal and recovery by short-chain polyaniline synthesized on jute fiber, J. Hazard. Mater., 162 (2009) 1086–1098.
[29] K. Vijayaraghavan, J. Jegan, K. Palanivelu, M. Velan, Batch and column removal of copper from aqueous solution using a brown marine alga *Turbinaria ornata*, Chem. Eng. J., 106 (2005) 177–184.
[30] G.S. Simate, S. Ndlovu, The removal of heavy metals in a packed bed column using immobilized cassava peel waste biomass, J. Ind. Eng. Chem., 21 (2015) 635–643.
[31] M. Ghasemi, A.R. Keshtkar, R. Dabbagh, S. Jaber Safdari, Biosorption of uranium(vi) from aqueous solutions by ca-pretreated *Cystoseira indica* alga: breakthrough curves studies and modeling, J. Hazard. Mater., 189 (2011) 141–149.
[32] İ.Y. Ipek, N. Kabay, M. Yüksel, Modeling of fixed bed column studies for removal of boron from geothermal water by selective chelating ion exchange resins, Desalination, 310 (2013) 151–157.
[33] K. Hristovski, P. Westerhoff, J. Crittenden, An approach for evaluating nanomaterials for use as packed bed adsorber media: a case study of arsenate removal by titanate nanofibers, J. Hazard. Mater., 156 (2008) 604–611.
[34] R. Han, Y. Wang, X. Zhao, Y. Wang, F. Xie, J. Cheng, M. Tang, Adsorption of methylene blue by phoenix tree leaf powder in a fixed-bed column: Experiments and prediction of breakthrough curves, Desalination, 245 (2009) 284–297.
[35] Z. Xu, J.-g. Cai, B.-c. Pan, Mathematically modeling fixed-bed adsorption in aqueous systems, J. Zhejiang Univ. Sci. A, 14 (2013) 155–176.
[36] Z. Aksu, F. Gönen, Biosorption of phenol by immobilized activated sludge in a continuous packed bed: prediction of breakthrough curves, Process Biochem., 39 (2004) 599–613.